

This is an electronic reprint of the original article. This reprint may differ from the original in pagination and typographic detail.

---

## The activation of C-O bonds in lignin Miscanthus over acidic heterogeneous catalysts

Samikannu, A; Mikkola, JP; Tirsoaga, A; Tofan, V; Fierascu, RC; Richel, A; Verziu, MN

*Published in:*  
Biomass Conversion and Biorefinery

*DOI:*  
[10.1007/s13399-022-03061-4](https://doi.org/10.1007/s13399-022-03061-4)

Published: 23/07/2022

*Document Version*  
Accepted author manuscript

*Document License*  
Publisher rights policy

[Link to publication](#)

*Please cite the original version:*  
Samikannu, A., Mikkola, JP., Tirsoaga, A., Tofan, V., Fierascu, RC., Richel, A., & Verziu, MN. (2022). The activation of C-O bonds in lignin Miscanthus over acidic heterogeneous catalysts: towards lignin depolymerisation to monomer units. *Biomass Conversion and Biorefinery*. <https://doi.org/10.1007/s13399-022-03061-4>

### General rights

Copyright and moral rights for the publications made accessible in the public portal are retained by the authors and/or other copyright owners and it is a condition of accessing publications that users recognise and abide by the legal requirements associated with these rights.

### Take down policy

If you believe that this document breaches copyright please contact us providing details, and we will remove access to the work immediately and investigate your claim.



**University Politehnica of Bucharest**

Faculty of Applied Chemistry and Materials Science

1-7 Gh Polizu Street, 011061, Bucharest, Romania

e-mail: [marian.verziu@upb.ro](mailto:marian.verziu@upb.ro)

---

April 19 , 2022

Biomass Conversion and Biorefinery  
Editor in Chief

Manuscript submission

**Title: The activation of C-C and C-O bonds in Lignin Miscanthus over acidic heterogeneous catalysts: Towards Lignin Depolymerisation to monomers units**

**Authors:** Ajaikumar Samikannu, Jyri Pekka Mikkola, Alina Tirsoaga, Vlad Tofan, Claudiu Fierascu, Aurore Richel, Marian Nicolae Verziu

Dear Prof. Martin Kaltschmitt,

Please find enclosed the files corresponding to the before-mentioned manuscript that we would like to submit to Biomass Conversion and Biorefinery for consideration as a Original Article. The lignin samples, extracted from Miscanthus plant both under acidic and basic conditions, were depolymerized over Ni and/or Nb-doped SBA-15 under hydrogen pressure. **The hexagonal ordering of a typically mesoporous SBA-15 was maintained after insertion of Ni and/or Nb as was highlighted by XRD analysis. In this study we showed that the presence of acidic sites, resulting from the insertion of Nb into SBA-15 structure, alongside of Ni sites promoted the activation of  $\beta$ -O-4 and C-C bonds from lignin samples leading to an increase in the yield of aromatic monomers.** The analysis of the reaction products carried out by LDI-TOF-MS and HPSEC techniques highlighted that the chemical composition of lignin samples played a very crucial role on catalytic performances activity of the catalysts.

In view of these performances, we think that the results will be of interest for a large audience of journal readers and, therefore, could reach the impact necessary for publication in Biomass Conversion and Biorefinery.

All authors are aware of the submission and agree to its publication. The work and the results presented in this manuscript are original, and they were not submitted for publication elsewhere.

Looking forward to hearing from you,

Sincerely,

Dr. Marian Verziu

Dr. Alina Tirsoaga

# The activation of C-C and C-O bonds in Lignin Miscanthus over acidic heterogeneous catalysts: Towards Lignin Depolymerisation to monomers units

Ajaikumar Samikannu<sup>a</sup>, Jyri Pekka Mikkola<sup>a,b</sup>, Alina Tirsoaga<sup>c,\*</sup>, Vlad Tofan<sup>d</sup>, Radu Claudiu Fierascu<sup>e,f</sup>, Aurore Richel<sup>g</sup>, Marian Nicolae Verziu<sup>h,\*</sup>

<sup>a</sup>Technical Chemistry, Department of Chemistry, Chemical-Biological Centre, Umeå University, SE-901 87, Umeå, Sweden

<sup>b</sup>Laboratory of Industrial Chemistry and Reaction Engineering, Johan Gadolin Process Chemistry Centre, Åbo Akademi University, Åbo-Turku, FI-20500, Finland

<sup>c</sup>Department of Physical Chemistry, Faculty of Chemistry, University of Bucharest, Bdul Regina Elisabeta, 4-12, Bucharest 030016, Romania

<sup>d</sup>Cantacuzino National Institute of R&D for Microbiology and Immunology, 103 Splaiul Independentei, Bucharest, 050096, Romania

<sup>e</sup>National Institute for Research & Development in Chemistry and Petrochemistry—ICECHIM, 202 Spl. Independentei, 060021 Bucharest, Romania

<sup>f</sup>Faculty of Chemical Engineering and Biotechnologies, University Politehnica of Bucharest, 1-7 Gh. Polizu Str., 011061 Bucharest, Romania

<sup>g</sup>Unit of Biological and Industrial Chemistry, University of Liege– Gembloux Agro-BioTech, Passage des Déportés, 2-B-5030 Gembloux, Belgium

<sup>h</sup>Department of Bioresources and Polymer Science, Advanced Polymer Materials Group, Faculty of Chemical Engineering and Biotechnologies, University Politehnica of Bucharest, 1-7 Gh Polizu Street, Bucharest, Romania

\*Corresponding author e-mail: tirsoaga@yahoo.com, marian.verziu@upb.ro

**Keywords** Lignin Miscanthus · Hydrogenolysis · Monomers · Methanol · Synergistic Effect

## Abstract

One-pot depolymerisation of lignin, extracted from Miscanthus plants under acidic (formic acid lignin, FAL) or basic conditions (ammonia lignin, AL), over Ni and/or Nb-doped SBA-15, was the subject of this study. The acid catalysts aforementioned prepared by sol-gel method were characterized by SEM-EDX, ATR-FTIR, Raman, XRD, N<sub>2</sub> adsorption/desorption isotherms and NH<sub>3</sub>-TPD techniques. The increase in acidity due to the insertion of Nb into SBA-15 structure promoted the selective cleavage of β-O-4 and C-C bonds from ammonia lignin leading to aromatic monomer yields up to 22 wt. % in 6h at 180 °C under 50 atm H<sub>2</sub>. The catalytic performances of Ni-Nb-SBA-15 as well as its stability were influenced by the chemical composition of the lignin sample as results of its extraction from Miscanthus plant.

## 1 Introduction

Lignocellulose represents the highest inedible renewable organic carbon resource with a yearly supply of approximately 200 billion tons [1]. Lignocellulosic materials mainly contains semi-crystalline polysaccharide cellulose (38–50%), amorphous polysaccharide hemicellulose (23–32%), and amorphous phenylpropanoid polymer lignin (15–25%) [2]. The lignin shows a very complex three-dimensional molecular structure composed by three monomers namely guaiacyl alcohol (G unit), syringyl alcohol (S unit) and *p*-coumaryl alcohol

(H unit) linked between each other by C-C or C-O ether bonds forming  $\beta$ -O-4,  $\alpha$ -O-4,  $\beta$ - $\beta$ , 5-5 and  $\beta$ -1 linkages. A wide range of lower molecular weight aromatic compounds can strategically be obtained from lignin valorization via/by the selective cleavage of these interunit linkages [3].

In the past decade the valorization of lignin was subjected to several processes which includes hydrogenolysis [4-6], oxidation [7], hydrolysis [8] and pyrolysis [9]. From the perspective of atom economy, hydrogenolysis was widely known for the production of aromatics from lignin [10]. Generally, heterogeneous catalysts based on transition metals are utilized to break the C-O linkage in lignin via interacting with hydrogen molecules. The prospective of lignin valorization extends for both deoxygenated and oxygenated products[11]. The completely deoxygenated products via HDO can be used as a renewable fuel in the transportation sector whereas a large variety of oxygenated products such as cyclohexa-none are used in the production of adipic acid. The selective cleavage of C-C or C-O bonds from structure of lignin as well as the reaction products distribution are influenced by the type of heterogeneous catalyst tested [12]. Recently, A. McVeigh *et al.* reported that the activation of alkyl-aryl bonds from lignin was more efficiently over rhodium than platinum catalyst [12]. The supported noble metal catalysts such as gold [13], platinum [14], palladium [15] or ruthenium [16] showed excellent performances in the hydrogenolysis of lignin to small molecules. Despite the superior performance of noble metals, high cost and limited availability render their commercialization unfeasible. On the other hand, cheap transition metal-based Ni catalysts show high activity for C-O bond cleavage as well as excellent chemoselectivity in aromatics production [17]. The efficiency granted by the presence of precious metals upon depolymerisation of lignin into aromatic monomers by cleavage of C-O bonds over NiM(noble metal) bimetallic catalysts was also reported [18].

The activation of C-O bond in lignin conversion is also influenced by the presence of Brönsted and Lewis acids sites. Y. Shao *et al.* reported the influence of some acid oxides such as Nb<sub>2</sub>O<sub>5</sub>, ZrO<sub>2</sub>, Al<sub>2</sub>O<sub>3</sub> and TiO<sub>2</sub> on the cleavage of C-O bond from pristine phenol. Thus, the disassociation energies for the C-O bond of adsorbed phenoxide decreased, from 5.76 to 4.41 eV on Nb<sub>2</sub>O<sub>5</sub>. Therefore, the Nb<sub>2</sub>O<sub>5</sub> species can carry out both a strong adsorption of phenol and thereby reducing the dissociation energy for C-O bonds [19]. The higher efficiency of Nb<sub>2</sub>O<sub>5</sub> support (Au/Nb<sub>2</sub>O<sub>5</sub>) compared with those aforementioned was highlighted by L. Dong *et al.* in the hydrodeoxygenation of lignin oil to valuable phenolics, in water, where a combination among the strong acidic sites, negatively charged Au clusters and the activation of the C-O bonds on NbO<sub>x</sub> species led to the yields of phenolics of 66.3 wt% from lignin oil [20].

The role of the acidity in the depolymerisation process of the lignin was highlighted by the use of Ni supported on silicates which showed a high catalytic activity in the lignin hydrogenolysis while the large surface area as well as the well-ordered pore structures of the of SBA-15 led to a minimization of the repolymerization [21]. The positive effect of mesostructured silica such as SBA-15 or MCM-41 in the reduction of char yield during depolymerisation of lignin process was also observed by Thepparat *et al.* [22].

Recently, W. Song *et al.* reported the efficiency of Ni-NbOx sites, obtained by supporting of Ni on Nb<sub>2</sub>O<sub>5</sub> in the hydrodeoxygenation of lignin-derived phenols to alcohols in aqueous phase [23].

In light of the above considerations, the aim of the present study was to investigate the influence of the acid sites of the catalyst in the distribution of reaction products and selectivity towards monomeric compounds achieved by the cleavage of C-O or C-C bonds between lignin units. The interest in the production of the aromatic monomers from lignin is motivated by their use in a wide range of the synthesis such as pesticides and pharmaceutical products. [Jean-Michel Lavoie, Wadou Baré, Mathieu Bilodeau, Depolymerization of steam-treated lignin for the production of green chemicals, *Bioresource Technology*, Volume 102, Issue 7, April 2011, Pages 4917-4920]. Herein, SBA-15 was used as support material due to its high surface area, the mesoporous structure in combination with high hydrothermal stability. The promotion of Nb and Ni over the supported SBA-15 was explored based on the state of art on lignin depolymerization. *Miscanthus x giganteus* was used as a feedstock for the extraction of lignin under acidic or basic conditions.

## 2. Experimental

### 2.1 Lignin extraction

The lignin tested in this study was extracted from *Miscanthus x giganteus* by soaking lignocellulosic raw material in aqueous ammonia solution for 6 h, at 60 °C, in a water bath (AL= ammonia lignin) or in formic acid/acetic acid/water mixture for 3 h at 107 °C (FAL=formic acid lignin) [24]. The recovery of lignin from the obtained black liquor was carried out by precipitation at pH=2 obtained either with sulfuric acid solution for AL or water for FAL, respectively. The success of lignin extraction was evidenced by the presence of β-O-4 bonds or aromatic C-O or C-C bonds in the structure of extracted material using NMR spectroscopy or by characteristic signals of aromatic ring vibrations of the phenylpropane groups recorded by FTIR spectroscopy [24].

### 2.2 Catalysts synthesis

All the chemicals included in this study were of reagent grade and purchased from Sigma-Aldrich. Nonionic Triblock-Copolymer Pluronic P<sub>123</sub> (EO<sub>20</sub>PO<sub>70</sub>EO<sub>20</sub>): Poly (ethylene glycol)-block-Poly (propylene glycol)-block-Poly (ethylene glycol) and tetraethyl orthosilicate (TEOS) were used as structure-directing agent and silica precursor, respectively. The other chemicals used for the preparation of modified SBA-15 mesoporous silica were hydrochloric acid (2M HCl aqueous solution) and Ni(NO<sub>3</sub>)<sub>2</sub>·6H<sub>2</sub>O and NbNC<sub>4</sub>H<sub>4</sub>·xH<sub>2</sub>O as Ni<sup>2+</sup> and Nb<sup>5+</sup> sources, respectively.

The mesoporous silica of SBA-15 type and metal ions containing SBA-15 materials were synthesized according to a classical procedure by a nonionic templating route under acidic conditions [25-28]. Two different metal ions (Ni<sup>2+</sup>, Nb<sup>5+</sup>) were incorporated into SBA-15 silica matrix by direct synthesis to prepare two M-SBA-15 catalysts, denoted as Ni-SBA-15 (Ni=5 wt.%) and Ni-Nb-SBA-15 (Si/Nb atomic ratio=40, Ni=5 wt.%), respectively.

### ***Ni-SBA-15 synthesis***

In a typical synthesis, 10 g of Pluronic P<sub>123</sub> was first dissolved in 70 ml of distilled water and 304 g of 2M HCl at 40°C for 4 h under stirring. Then, 21.4 g of TEOS was added to the clear surfactant solution followed by the addition of an appropriate amount of nickel nitrate dissolved in distilled water. The obtained reactants mixture was maintained at 40 °C for 20 h under vigorous stirring. The molar composition of the resulting mixture (pH 0.5-1.0) was the following: TEOS-P<sub>123</sub>-HCl-Ni-H<sub>2</sub>O:1.0-0.17-5.72-0.05-193. The homogeneous synthesis mixture was transferred into a polypropylene bottle and aged at 90°C for 48 h under static conditions. The resulting material was then filtered off, thoroughly washed with distilled water and dried in air at room temperature for 20 h. Finally, the as-synthesized material was calcined in air at 550 °C for 8 h using a heating rate of 1°C/min. in order to remove the surfactant template.

### ***Ni-Nb-SBA-15 synthesis***

Ni-Nb-SBA-15 sample was synthesized by niobium ammonium oxalate-nickel nitrate incorporation during the formation of mesostructured silica following the procedure described above for the synthesis of Ni-SBA-15 sample. Aqueous solutions of required amounts of Nb<sup>5+</sup> and Ni<sup>2+</sup> precursors were incorporated into the reagents' mixture (surfactant-silicate) after TEOS was added. The obtained synthesis mixture (pH 0.5-1.0) had the following molar composition: TEOS-P<sub>123</sub>-HCl-Nb-Ni-H<sub>2</sub>O:1.0-0.17-5.72-0.025-0.05-193. All the subsequent synthesis steps were kept as described above according to Ni-SBA-15 synthesis.

### 2.3 Catalysts characterization

The adsorption-desorption isotherms were recorded on a micromeritics ASAP 2010 at  $-196\text{ }^{\circ}\text{C}$  after outgassing the samples at  $120\text{ }^{\circ}\text{C}$  K for 3 h. The specific surface areas were calculated using the BET method and the pore volumes were calculated from the corresponding desorption isotherms. The pore size distributions were estimated using the Barrett, Joyner and Halenda (BJH) algorithm using the built-in software from Micromeritics.

The XRD patterns were recorded using Bruker D8 Discover equipment (Bruker AXS, Karlsruhe, Germany) ( $\text{Cu}_{\text{K}\alpha 1}$   $\lambda = 1.5406\text{ \AA}$ ), between  $0.4$  and  $70^{\circ}$  ( $2\theta$ ),

Total surface acidity of the catalysts was determined by means of the temperature-programmed desorption method (TPD) on a BELCAT II instrument (MicrotracBEL Corp.). For all acidity measurements, 5 %  $\text{NH}_3$  in He was used as a probe molecule. In a typical measurement, about  $\sim 50$  mg of the sample was placed in an adsorption vessel and the sample was evacuated at  $550\text{ }^{\circ}\text{C}$  for 2 h under He flow. Subsequently, the sample was cooled down to  $50\text{ }^{\circ}\text{C}$ , the catalyst was saturated with 5%  $\text{NH}_3$  in He for 0.5 h and subsequently flushed with He at  $100\text{ }^{\circ}\text{C}$  for 1 h, to remove traces of physisorbed  $\text{NH}_3$ , TPD was carried out from  $100$  to  $450\text{ }^{\circ}\text{C}$ , at a heating rate of  $10\text{ }^{\circ}\text{C}/\text{min}$  under He flow. After each measurement, the amount of chemisorbed/desorbed  $\text{NH}_3$  was determined from the calibration curves obtained from varying volumes of  $\text{NH}_3$  in He. The relative contribution of individual acid sites (weak, medium and strong) was obtained by deconvolution of the TPD profiles using the inbuilt ChemMaster software (version 1.4.19, MicrotracBEL), a multiple-Gaussian function was selected for fitting the experimental TPD data. Further, for determining the strength of acid sites, the activation energy ( $E_a$ ) of  $\text{NH}_3$  desorption from the acid sites, were also calculated by performing  $\text{NH}_3$ -TPD experiments at different heating/desorption rates ( $5\text{--}30\text{ }^{\circ}\text{C}/\text{min}$ ) while keeping the sample mass and inert gas flow rate constant.

The surface morphology and elemental composition of the catalytic materials were examined by field-emission scanning electron microscopy (FESEM, Carl Zeiss Merlin GmbH) operating at 5 kV, equipped with energy-dispersive X-ray spectroscopy (EDS, Oxford Instruments X-MAX 80  $\text{mm}^2$ ).

FTIR measurements were done on a Vertex 70 Bruker FTIR spectrometer (USA), equipped with an attenuated total reflectance (ATR) accessory. For each sample 32 scans were registered in the ATR-FTIR mode, at room temperature and a resolution of  $4\text{ cm}^{-1}$  in  $600\text{--}4000\text{ cm}^{-1}$  wavenumber region.

Raman analysis was carried out using a Renishaw inVia Confocal Raman microscope system. The excitation laser wavelength was 473 nm. The Raman spectra were acquired in the



extended spectral region from 100 to 3200  $\text{cm}^{-1}$ . Raman studies were carried out under ambient conditions and the region analyzed was from 100 to 900  $\text{cm}^{-1}$ .

## 2.4 Catalytic tests

Typical depolymerisation experiments were carried out in autoclave conditions using 0.5 g lignin and 0.1 or 0.3 g catalyst in 70 mL methanol, for 3 or 6 h, at 180 °C, under 50 bar of  $\text{H}_2$  and vigorous stirring. After reaction, the unreacted lignin was recovered by the centrifugation of the mixture at 15.000 rpm for 10 min. The conversion of lignin to low molecular weight compounds as well as the yield were calculated using Eq. (1) and Eq.(2):

$$C\% = \frac{m_i - m_f}{m_i} \times 100 \quad (1)$$

$$\text{Yield}(\%) = \frac{\text{Selectivity}(\%) \times \text{Conversion}(\%)}{100} \quad (2)$$

Where:  $m_i$  = mass of lignin introduced in reaction

$m_f$  = mass of lignin recovered after reaction

The catalyst was recycled for three consecutive runs. After the first run, the catalyst and the remaining lignin were centrifuged and dried. Fresh lignin and methanol were added to the initial mixture and used for the next run under similar conditions.

Analysis of the reaction products was performed by recording the high-resolution mass spectra with an Ultraflex LDI-TOF-MS (matrix-assisted laser desorption/ionization- time of flight-mass spectrometry) (Bruker Daltonic) operating in the reflector and linear positive or negative mode using a pulsed nitrogen laser.

The peak average molecular mass distribution of lignin was evaluated by using a High-Performance Size Exclusion Chromatography (HPSEC) with UV detection at 280 nm. The system was composed of a Waters 2690 Alliance chromatograph, coupled to a Waters 996 UV detector (both from Waters Corp., Milford, MA, USA), and equipped with a TSK-Gel PWxl guard column and two TSKgel G3000PWXL columns (300 mm  $\times$  7.8 mm I.D.) in series (with 7 and then 6  $\mu\text{m}$  particle diameters, respectively) (Tosoh Bioscience, Tessenderlo, Belgium).

A polynomial calibration curve was established by using a range of narrow distribution poly(4-styrenesulfonic acid) ammonium salt (PSS-Na) (Sigma-Aldrich, Diegem, Belgium) with average molecular masses from 208 Da to 77.4 kDa. The eluent solution contained 6.9 g

$\text{NaH}_2\text{PO}_4 \cdot \text{H}_2\text{O}$  and 3.2 g NaOH in distilled water and the pH was adjusted to 12 with 6 M NaOH. The flow rate was 0.9 mL/min, at a temperature of 30 °C. Before use, it was filtrated over 0.45  $\mu\text{m}$  filter and sonicated for 15 min. PSS-Na and lignins were dissolved in a volume of eluent, 1 mg/mL and 3 mg/mL, respectively. Before analyses, the lignin solutions were kept under magnetic stirring during 48 h to ensure a complete dissolution, and filtered through a 0.45  $\mu\text{m}$  MCE membrane prior to injection.

Analyses of phenolic compounds were carried by GC–MS, i.e. gas chromatography (HP GC System 6890 Series) coupled to mass spectrometry (HP Mass Selective Detector 5973) (Agilent Technologies, Diegem, Belgium). Separation was done on an Agilent J&W capillary column (FactorFour VF–5 ms, 30 m  $\times$  0.25 mm ID, 0.25  $\mu\text{m}$  film thickness). Helium was used as carrier gas at a flow rate of 1 mL  $\text{min}^{-1}$ . Injection chamber was set at 250 °C, and the temperature program was 8 min at 40 °C, followed by a linear increase at 5 °C  $\text{min}^{-1}$  to 250 °C and then at 2 °C  $\text{min}^{-1}$  to 300 °C which was maintained for 20 min. Compounds were detected using a flame ionization detector at 320 °C.

### 3 Results and discussion

#### 3.1 Catalysts characterization

The  $\text{N}_2$  adsorption-desorption isotherms as well as the textural characteristics of the SBA-15 based materials prepared are presented in the Fig. 1 and Table 1, respectively. All undoped or doped SBA-15 samples showed a Type IV hysteresis (Fig.1) characteristic for mesoporous materials with a cylindrical pore geometry [29]. The morphology of SBA-15 was stable despite the deposition of Ni and Nb, as shown in Fig. 2. The porous nature of SBA-15 allows the deposition of Ni and Nb, as evidenced by the decrease in surface area and pore size. Interestingly, a small decrement in surface area was observed after the deposition of Ni on SBA-15. This can be attributed to the partial blockage of pores and channels of SBA-15. As shown in Tabel 1, micropores of SBA-15 were preferentially occupied which led to a shift in pore size distribution from 5.9 nm to 5.7 nm. On the other hand, the surface area decreased drastically from 863 to 680  $\text{m}^2/\text{g}$  after the incorporation of Ni and Nb. Unlike Ni, the preferential deposition zone for Nb is on the outer surface of SBA-15. The smooth and bloated SBA-15 as shown in Fig 2b reveals the deposition of Nb on the outer surface/edges of the SBA. Overall pore size distribution of Ni/SBA-15 and Ni-Nb/SBA-15 still agrees with the mesoporous nature of SBA-15. However, the hysteresis loop of modified SBA-15 is altered especially in the case of NiNb/SBA-15.

**Table 1** Textural characteristics of the investigated catalysts

Catalyst	$S_{\text{BET}}$ ( $\text{m}^2/\text{g}$ )	$S_{\text{Micro}}$ ( $\text{m}^2/\text{g}$ )	$S_{\text{Micro}}/S_{\text{BET}}$ (%)	Pore size (nm)
SBA-15	863	131	15	5.9
Ni-SBA-15	783	95	12	5.5
Ni-Nb-SBA-15	680	78	11	5.7

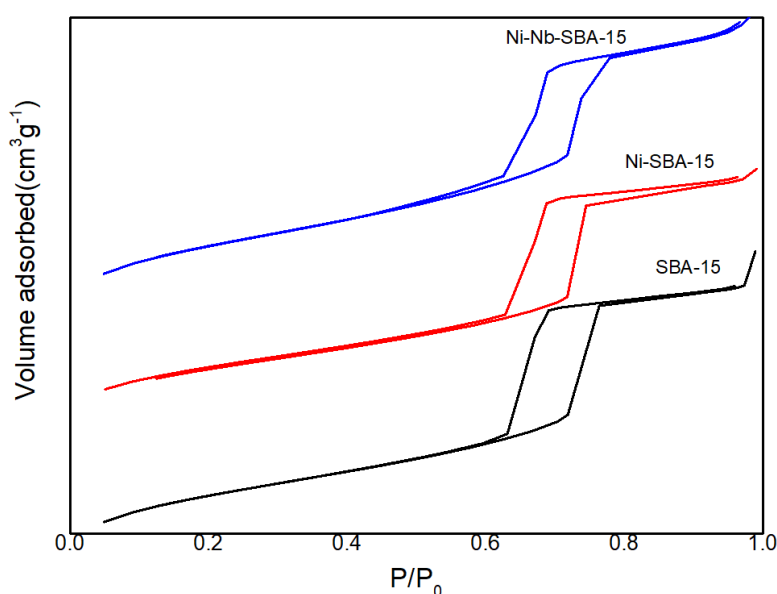


**Fig. 1**  $\text{N}_2$  adsorption-desorption isotherms of doped and undoped SBA-15

The pristine morphology of SBA-15 is in a rod-like shape, as shown in Fig. 2a. The particle size distribution ranged from 500 to 1200 nm. The incorporation of Ni and Nb into the framework also gives a similar worm-like morphology as well as the breakage of rope-like domains that might be due to distortion because of differences in bond length and bond angles of Si-O-Ni and Si-O-Nb compared to Si-O-Si. The presence of Ni and Nb is also evidenced from the EDX mapping as shown in Fig. 2. Unlike the impregnation technique, Ni and Nb were deposited atomically during the synthesis protocols of SBA-15. Therefore, the EDX analysis revealed slightly lower metal loading compared to theoretical metal loading.

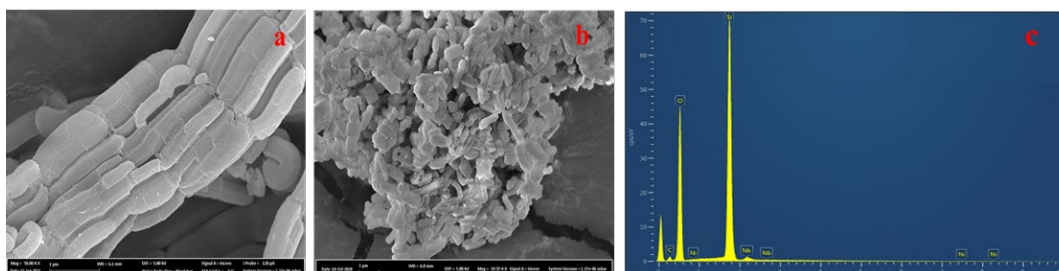


**Fig. 2** SEM images of a) SBA-15; b) Ni-Nb-SBA-15 and c) EDX for Ni-Nb-SBA-15

Low-angle XRD of the doped SBA-15 showed the diffraction lines at  $2\Theta=0.90, 1.50$  and  $1.70$ , characteristic for hexagonally ordered of a typically mesoporous SBA-15 (Fig. S1) [Michal Kruk and Mietek Jaroniec, Characterization of the Porous Structure of SBA-15, Chem. Mater. 2000, 12, 1961-1968]. The insertion of Nb besides Ni into SBA-15 structure led to a small shift towards higher angles of the position of the (100) plane (Fig. S1) which could be due to a small disorder of the mesoporous structure [Monickarla Teixeira Pegado da Silva, Felipe Fernandes Barbosa, Marco Antonio Morales Torre, Jhonny Villarroel-Rocha, Karim Sapag, Sibebe B. C. Pergher and Tiago Pinheiro Braga, Synthesis of Fe<sub>2</sub>SiO<sub>4</sub>-Fe<sub>7</sub>Co<sub>3</sub> Nanocomposite Dispersed in the Mesoporous SBA-15: Application as Magnetically Separable Adsorbent, Molecules 2020, 25, 1016]

ATR-FTIR spectra of the doped and undoped SBA-15 are depicted in Fig. 3. The characteristics IR band of SBA-15 are highlighted at  $1065, 962$  and  $807$   $\text{cm}^{-1}$ , respectively, which correspond to Si-O-Si asymmetrical stretching, SiO<sub>4</sub> tetrahedron ring and Si-OH stretching [30], respectively and these were also noticed in doped SBA-15. However, a significant decrease in the intensity of Si-O-Si absorption band at  $1065$   $\text{cm}^{-1}$  was observed. This decrease could be correlated with the formation of new bonds Si-O-Ni or/and Si-O-Nb, as shown in Fig. 3. The EDX mapping and SEM images further support the interaction of Ni and Nb with SBA-15.

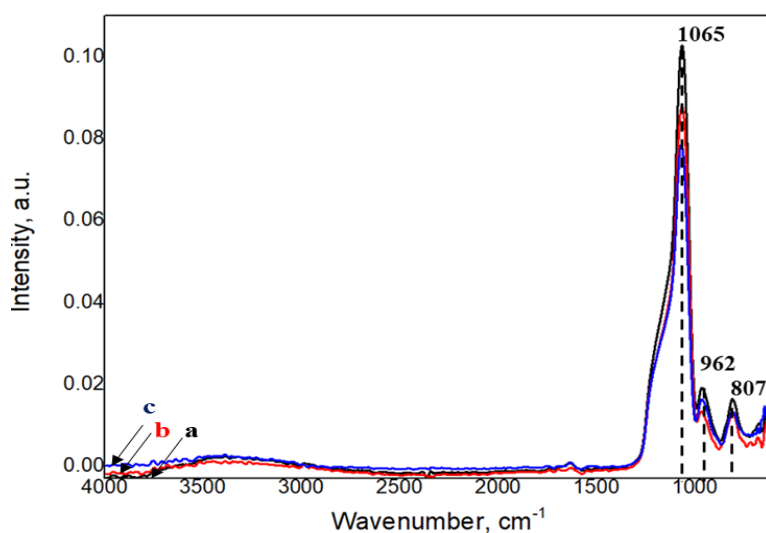


**Fig. 3** ATR-FTIR spectra for: a) SBA-15; b) Ni-SBA-15 and c) Ni-Nb-SBA-15

Different surface metal oxides can be identified from Raman spectroscopy which is a powerful tool to get insights into the structure and bond of metal oxides [31]. The Raman bands at  $573$  and  $647$   $\text{cm}^{-1}$  are assigned to distorted NbO<sub>6</sub> octahedra while the band at  $815$   $\text{cm}^{-1}$  could correspond to both regular tetrahedral NbO<sub>4</sub> structures [32] and Ni-Nb-O bond [33] (Fig. 4).

Furthermore the degree of distortion of octahedral NbO<sub>6</sub> can lead to weak Brönsted acidity (slightly distorted octahedral NbO<sub>6</sub>) or strong Lewis acidity (highly distorted octahedral NbO<sub>6</sub> species with Nb=O bond ) [34].

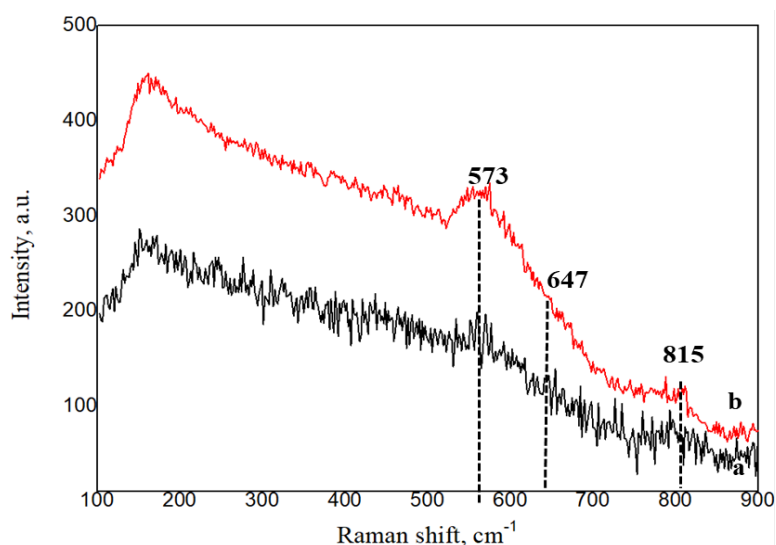


**Fig. 4** Raman spectra for a) Ni-SBA-15 and b) Ni-Nb-SBA-15

The NH<sub>3</sub>-TPD measurements of doped and undoped SBA-15 materials show the presence of acidic sites with varying strengths. The broad distribution of desorption from 100 °C to 550 °C showed also the presence of acidic sites with weak (100 °C-200 °C), medium (200 °C-400 °C) and strong (> 400 °C) strengths (Fig. 5).

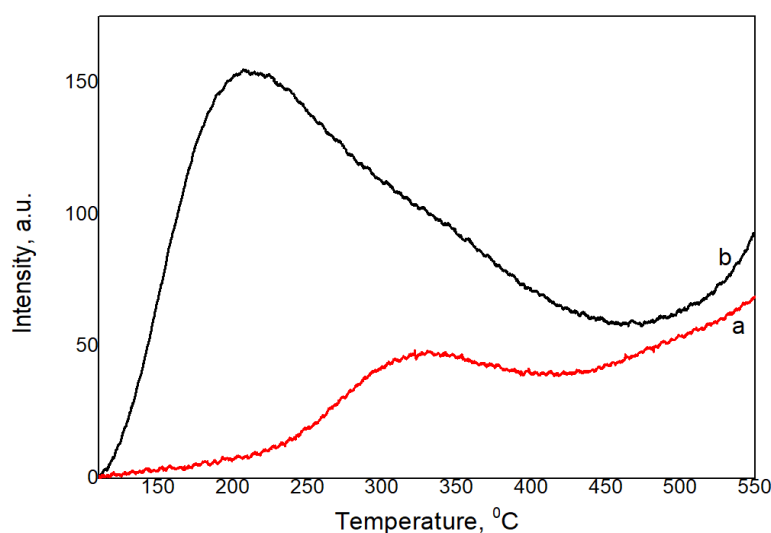


**Fig. 5** NH<sub>3</sub>-TPD profiles for a) Ni-SBA-15 and b) Ni-Nb-SBA-15

The insertion of Nb into SBA-15 structure led to an increase in moderate acid sites concentration from 52 (for Ni-SBA-15) to 102 μmol/g (for Ni-Nb-SBA-15) (Tabel 2) .

**Table 2** Total amount and density of acid sites for doped SBA-15

Catalyst	Total amount of acid sites ( $\mu\text{mol/g}$ )	Acidic sites density ( $\mu\text{mol/m}^2$ )
Ni-SBA-15	52	0.06
Ni-Nb-SBA-15	102	0.15

### 3.2 Catalytic behavior

The catalytic performances of the Nb doped/undoped Ni-SBA-15 in the depolymerisation of lignin extracted in acid or basic conditions were evaluated by several techniques such as LDI-TOF-MS, HPCSEC and GC-MS.

In this work, LDI-TOF-MS measurements (recorded in both positive and negative ion modes) were carried out to estimate the molecular weight distribution pattern of the constitutive fragments due to a depolymerisation process of formic acid (FAL) and ammonia-lignin (AL) extracted from *Miscanthus x giganteus* [24] over Ni-SBA-15 and Ni-Nb-SBA-15 catalysts. However, the ionisation in the negative ion mode led to a higher quality spectra than those corresponding to positive ion mode and we decided to use these spectra in order to estimate the molecular weight of the compounds resulted after lignin depolymerisation.

The structure of lignin shows a lot of aromatic ether C-O bonds and the selective cleavage of these bonds plays a major role in its valorisation. Although the catalytic activity Ni based catalyst in the cleavage C-O bonds from lignin model compounds is well known [11], the complexity, heterogeneity of the lignin structure as well as its purity can influence the catalytic performances in the depolymerisation process. On the other hand, there is a difference between formic acid and ammonia lignin samples both in terms of C-C and  $\beta$ -O-4 linkages which connect the phenylpropane units ( $\beta$ -O-4 linkages are predominant in structure of AL) and of purity, the content of carbohydrates in AL is higher than in FAL [24].

The HPSEC analysis highlighted that the presence of niobium along that of nickel into SBA-15 structure led to an improve of AL depolymerisation to low molecular weight compounds (Fig. 6) when we compared than with Ni-SBA-15 due to the reduction of activation energy of C-O bonds as a result of its absorption on  $\text{Nb}_2\text{O}_5$  [19]. Moreover, the generation of Brønsted and Lewis acid sites (Figure 4) as well as the increase in the moderate acidity of SBA-15 (Tabel 4) as a result of Nb insertion into SBA-15 structure (Table 4) could significantly promote the cleavage of  $\beta$ -O-4 and  $\alpha$ -O-4 ether linkages [35]. On the other hand nickel-supported hydrotalcite showed a good catalytic activity in the deconstruction of a lignin model compound such as 2-phenoxy-1-phenethanol which contains  $\beta$ -O-4 alkyl-aryl-ether bond, the

most abundant intermonomer bond in native lignin [36]. Therefore, there is a synergetic effect between Ni and Nb for depolymerisation of lignin into monomers (range of  $m/z$  50-200, Fig. 6).

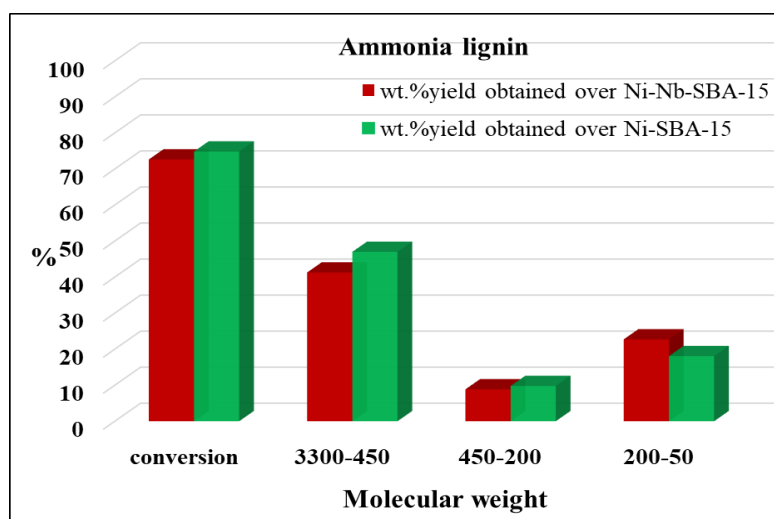


**Fig. 6** Depolymerisation of ammonia lignin under autoclave conditions (0.1g catalyst, 0.5 g ammonia lignin, 70 mL methanol, 50 bars  $H_2$ , 180 °C, 6 h).

Active hydrogen generated by the interaction between nickel-based catalysts and alcohol will attack the C-O bonds in lignin and the recondensation reactions between lignin fragments can be avoided, leading to an increase in yields of monomeric phenols [37]. On the other hand, methanol can act as the nucleophilic reagent for C-O-C cleavage in alcoholysis reaction [17] and oxophilicity of  $Nb_2O_5$  promoted the cleavage of C-O bonds leading to yields of around 30 wt.% aromatic alcohols as a result of catalytic hydrogenolysis of Kraft lignin over 5Ni-5Re/ $Nb_2O_5$  at 330°C for 3h [39]. Therefore, the cleavage of C-O bonds over acid catalyst as well as the catalytic performance of Ni-based catalyst in the selective hydrogenolysis of C-O bond [38] to promote a strong synergetic effect between Ni and Nb in depolymerisation of AL to low molecular weight compounds. This effect was also very well highlighted by LDI-TOF-MS analysis where the presence of Nb led to the formation of mono and dimers compounds (Fig S3).

In accordance with the literature [40] the LDI-TOF-MS spectrum of the supernatant recovered after lignin depolymerisation process could be divided in three distinguished groups of peaks which correspond to monomers (range of  $m/z$  74-250), dimers (range of  $m/z$  250-450) and tri- and tetramers (range of  $m/z$  450-840), respectively. **Because no dimeric structures with a mass of less than 250 Da have been reported, a clear delimitation between the monomer and**

dimer domains has to be accepted, but a sharp mass cut-off is unreasonable to be used to discriminate between trimers, tetramers and higher order oligomers [Jarrell TM, Marcum CL, Sheng H, Owen BC, O'Lenick CJ, Maraun H, J.J. Bozell, H.I. Kenttamaa. Characterization of organosolv switchgrass lignin by using high performance liquid chromatography/high resolution tandem mass spectrometry using hydroxide-doped negative-ion mode electrospray ionization. *Green Chem.* 2014;16(5):2713–27].

It is well accepted that the heterogeneous lignin biopolymer in grasses is formed mainly of three monolignol structural units (such as p-coumaryl alcohol (H), coniferyl alcohol (G) and sinapyl alcohol (S)), which each have three carbon atoms in the side chain. However, following a depolymerisation process of Kraft lignin, J. Prothmann *et al.* found an oligomer derived from lignin with 3-buten-1-ol moiety linked to an aromatic ring (of  $m/z$  316;  $C_{18}H_{20}O_5$ ) by using UHPLC/HRMS<sup>n</sup> approach [Jens Prothmann, Peter Spiegel, Margareta Sandhal, Charlotta Turner, Identification of lignin oligomers in Kraft lignin using ultra-high-performance liquid chromatography/high-resolution multiple-stage tandem mass spectrometry (UHPLC/HRMS<sup>n</sup>). *Analytical and Bioanalytical Chemistry* (2018) 410:7803-7814]. Furthermore, M. Bergs *et al.*, reported a G-type monomer with n-butyl moiety (zingerone,  $C_{11}H_{16}O_2$ ) as a degradation product of organosolv lignin isolated from *Miscanthus* species [Michael Bergs, Xuan Tung Do, Jessica Rumpf, Peter Kusch, Yulia Monakhova, Christopher Konow, Georg Volkering, Ralf Pude, Margit Schulze; Comparing chemical composition and lignin structure of *Miscanthus x giganteus* and *Miscanthus nagara* harvested in autumn and spring and separated into stems and leaves. *RCS Advances*, 2020, 10, 10740-10751]. Besides, O. Kriger *et al.* reported molecular fragments of lignin oligomers extracted from a pretreatment of *Miscanthus* plant with the TFA/H<sub>2</sub>O<sub>2</sub> system and having 3-hydroxy-tetrahydrofuran group attached to an aromatic ring of a monolignol structural unit [Olga Kriger, Ekaterina Budenkova, Olga Babich, Stanislav Suhii, Nikolay Patyukov, Yakov Masyutin, Vyacheslav Dolganuk, Evgeny Chupkhin, The process of producing bioethanol from delignified cellulose isolated from plants of the *Miscanthus* genus, *Bioengineering*, 2020, 7, 61, 6-11].

Typically pinoresinol structures are formed by  $\beta$ - $\beta$  coupling of two coniferyl alcohol monomers following by a re-aromatization process; however  $\beta$ - $\beta$  coupling of monolignols can occur with the formation of tetrahydrofuran structures [Judith Schafer, Melinda Sattler, Yasir Iqbal, Iris Lewandowski, Mirko Bunzel, Characterization of *Miscanthus* cell wall polymers; *GCB Bioenergy*, 2019, 11, 191-205], due to the acylated monolignols which participates in the formation of lignin biopolymer by conventional radical coupling process. [Fachuang Lu, John Ralph, Novel tetrahydrofuran structures derived from  $\beta$ - $\beta$ -coupling reactions involving sinapyl

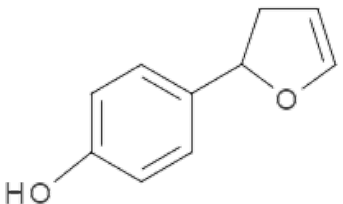
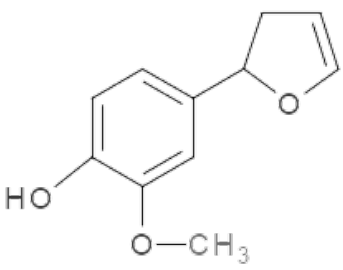
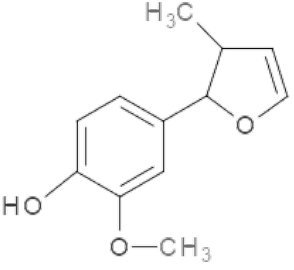
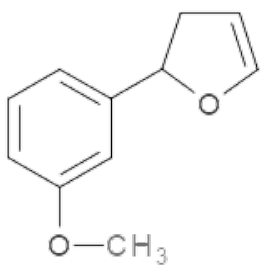


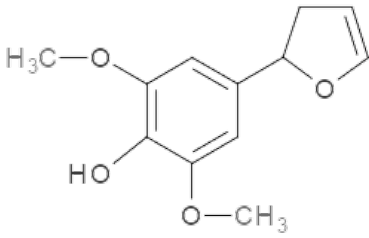
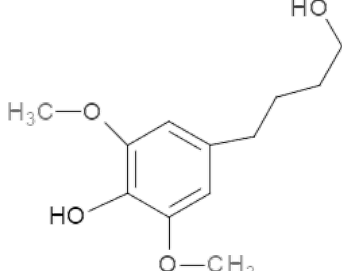
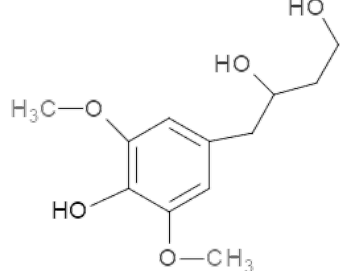
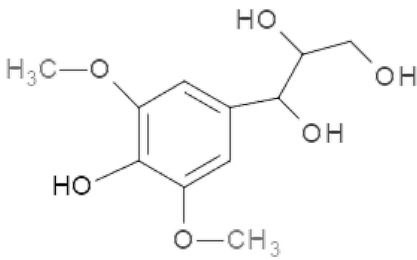
acetate in Kenaf lignins, *Organic and Biomolecular Chemistry*, 2008, 6, 3681-3694.]. Based on the degradation products isolated from a catalytic hydrogenolysis process of lignin, A. Sakakibara proposed a structural model of softwood lignin which contains tetrahydrofuran-derived units as possible structures presented in the lignin polymer [A Sakakibara, A structural model of softwood lignin; *Wood Sci Technol*, 1980, 14, 89-100]. Therefore, our mass spectra revealed peaks that can be attributed to monomeric structures with moieties of three or four carbon atoms, which are in line with the fragments reported by S.K. Saito *et al.* [40 - S.K. Saito, T. Kato, H. Takamori, T. Kishimoto, K. Fukushima; A new analysis of the depolymerized fragments of lignin polymer using ToF-SIMS; *Biomacromolecules*, 6 (2005), pp. 2688-2696] derived from a pinosresinol structure.

The most abundant related-monomeric compounds observed from the mass spectrum (Figure S1b) of the depolymerised AL sample over Ni-SBA-15 catalyst for 6h were derived from (H) p-hydroxyphenyl (m/z of 162), (G) guaiacyl (m/z of 176, 192, 206) units and from (S) syringyl (m/z of 222, 226, 242, 244) units as reported by S.K. Saito *et al.* [41] which differ from each other by 14-17 Da. These differences correspond to different numbers of O atoms/CH<sub>2</sub>/CH<sub>3</sub>/OH groups presented in the molecular structures (Table 3). Due to a different reactivity between lignin units, H and G-units are less present in the spectrum because they can be easily repolymerized [42]. Furthermore, the peaks at m/z of 110 and m/z of 112 were observed on the mass spectra and they were assigned to catechol and cyclotene, respectively as reported by E. Christensen *et al.* [43]. The heterogeneity of the lignin sample is also evidenced by the structures of the dimeric species with m/z of 246, 260, 272, 298, 312, 326, 340, 358, 360, 374, 446 and 460 that could be related to the different linkages between the monomeric units of the lignin primarily of phenylcoumaran- and resinol-type structures [44], as well as to different numbers of CH<sub>2</sub>/OH groups presented in the molecule structure [45]. The m/z of 272 Da peak might be also attributed to diarylpropane – and biphenyl-type structures (with all R=H), while the m/z of 260 and 246 Da peaks might be attributed to a diphenyl structure (Table 4) [45]. If the presence of Nb which promotes the cleavage of C<sub>aromatic</sub>-C bonds [46] led to the diminishing of peak intensity with m/z for 311 and 325 over Ni-Nb-SBA-15 (Fig. S3) in comparison with Ni-SBA-15, the stability of compounds with m/z of 373, 374 (Fig S3) could be due to the steric effect [47] of -OCH<sub>3</sub>, -CH<sub>2</sub>-OH and -C<sub>3</sub>H<sub>7</sub>, substituents on the phenylcoumaran (Table 4). In accordance with the literature reports, it might be possible to assign dimers with β-O-4 linkages to peaks with m/z of 329 [48] and 375 [49], respectively. It is well known that it is difficult to establish trimeric and tetrameric structures due to the repolymerisation process, but some trimers and tetramers were highlighted from the mass spectrum at m/z of 560, 574,

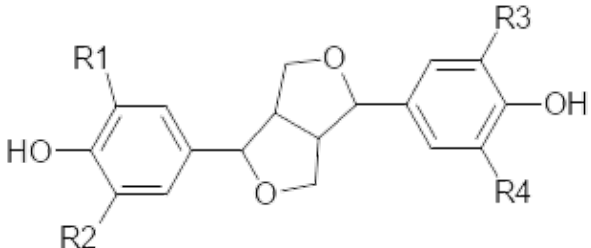
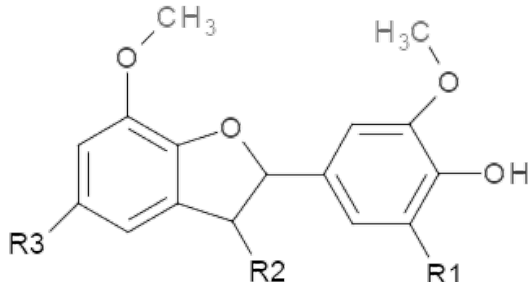
588, 602 and 635, respectively, that could be assigned to GGG, GGG, GSG, GGS and GGSG type structures with different linkages, according to the relevant literature [44, 50,51]. Therefore, the insertion of the Nb and Ni into SBA-15 structure promoted the cleavage of lignin linkages and so a bimodal distribution of the lignin-related compounds was highlighted from the mass spectrum (Figure S1a): monomers (with dominant molecular mass signal, m/z of 162, 222, 242, 244) and dimers (with dominant molecular mass signals m/z of 260, 272, 312, 326, 374, 376) with different resinol-, phenylcoumaran- and diphenyl-type structures. Furthermore dimers with  $\beta$ -O-4 linkages were identified on the spectra as small peaks with m/z of 359 [48], 375 [49] (it is the most valuable peak due to S/N value), 378 [52], respectively, as reported in the literature. The chemical structure of monomer and dimer compounds [41,45,53] are shown in the table 3 and 4 respectively.

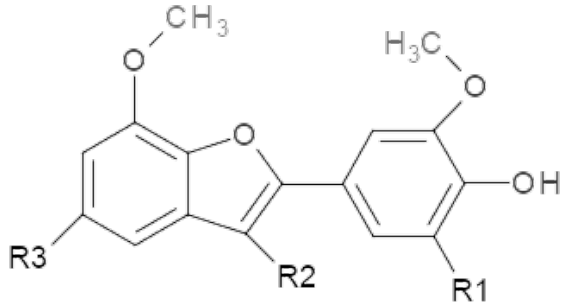
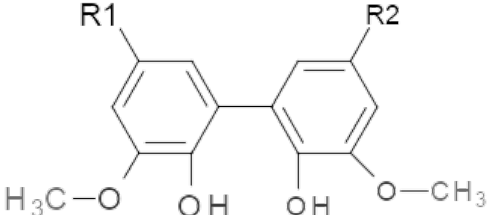
**Table 3** Possible type-structures of monomeric components from AL lignin depolymerisation process (with their elemental compositions): A) p-Hydroxyphenyl, B) Guaiacyl, C) Syringyl - derivatives

<b>A) p-Hydroxyphenyl-derivatives</b>		
		
<b>162 Da (C<sub>10</sub>H<sub>10</sub>O<sub>2</sub>)</b>		
<b>B) Guaiacyl-derivatives</b>		
		
<b>192 Da (C<sub>11</sub>H<sub>12</sub>O<sub>3</sub>);</b>	<b>206 Da (C<sub>12</sub>H<sub>14</sub>O<sub>3</sub>)</b>	<b>176 Da (C<sub>11</sub>H<sub>12</sub>O<sub>2</sub>)</b>
<b>C) Syringyl derivatives</b>		

 <p><b>222 Da (C<sub>12</sub>H<sub>14</sub>O<sub>4</sub>)</b></p>	 <p><b>226 Da (C<sub>12</sub>H<sub>18</sub>O<sub>4</sub>)</b></p>	 <p><b>242 Da (C<sub>12</sub>H<sub>18</sub>O<sub>5</sub>)</b></p>
 <p><b>244 Da (C<sub>11</sub>H<sub>16</sub>O<sub>6</sub>)</b></p>		

**Table 4** Possible type-structures of dimeric components from lignin depolymerisation process (with their elemental compositions): A) resinol, B) phenylcoumaran

Possible dimer type-structures	Molar mass (Da)
<p><b>A) resinol</b></p> 	<p>298 = {R<sub>1</sub>=R<sub>2</sub>=R<sub>3</sub>=R<sub>4</sub>=H}, C<sub>18</sub>H<sub>18</sub>O<sub>4</sub>            340 = {R<sub>1</sub>=R<sub>2</sub>=R<sub>3</sub>=H; R<sub>4</sub>=OC<sub>2</sub>H<sub>3</sub>}, C<sub>20</sub>H<sub>20</sub>O<sub>5</sub>            358 = {R<sub>1</sub>=R<sub>3</sub>=H; R<sub>2</sub>=R<sub>4</sub>=OCH<sub>3</sub>}, C<sub>20</sub>H<sub>22</sub>O<sub>6</sub>            446 = {R<sub>1</sub>=R<sub>3</sub>=OCH<sub>3</sub>; R<sub>2</sub>=R<sub>4</sub>=OC<sub>2</sub>H<sub>5</sub>}, C<sub>24</sub>H<sub>30</sub>O<sub>8</sub>            460 = {R<sub>1</sub>=OCH<sub>3</sub>; R<sub>2</sub>=R<sub>3</sub>=R<sub>4</sub>=OC<sub>2</sub>H<sub>5</sub>}, C<sub>25</sub>H<sub>32</sub>O<sub>8</sub></p>
<p><b>B) phenylcoumaran</b></p> 	<p>272 = {R<sub>1</sub>=R<sub>2</sub>=R<sub>3</sub>=H}, C<sub>16</sub>H<sub>17</sub>O<sub>4</sub>            358 = {R<sub>1</sub>=OCH<sub>3</sub>; R<sub>2</sub>=H; R<sub>3</sub>=OC<sub>3</sub>H<sub>5</sub>}, C<sub>20</sub>H<sub>22</sub>O<sub>6</sub>            360 = {R<sub>1</sub>=OCH<sub>3</sub>; R<sub>2</sub>=CH<sub>2</sub>OH; R<sub>3</sub>=C<sub>2</sub>H<sub>5</sub>}, C<sub>20</sub>H<sub>22</sub>O<sub>6</sub>            374 = {R<sub>1</sub>=OCH<sub>3</sub>; R<sub>2</sub>=CH<sub>2</sub>OH; R<sub>3</sub>=C<sub>3</sub>H<sub>7</sub>}, C<sub>21</sub>H<sub>26</sub>O<sub>6</sub></p>
<p><b>B') phenylcoumaran</b></p>	<p>298 = {R<sub>1</sub>=C<sub>2</sub>H<sub>5</sub>; R<sub>2</sub>=R<sub>3</sub>=H}, C<sub>18</sub>H<sub>18</sub>O<sub>4</sub>            312 = {R<sub>1</sub>=OC<sub>2</sub>H<sub>3</sub>; R<sub>2</sub>=R<sub>3</sub>=H}, C<sub>18</sub>H<sub>16</sub>O<sub>5</sub>            326 = {R<sub>1</sub>=OC<sub>3</sub>H<sub>5</sub>; R<sub>2</sub>=R<sub>3</sub>=H}, C<sub>19</sub>H<sub>18</sub>O<sub>5</sub>            330 = {R<sub>1</sub>=OCH<sub>3</sub>; R<sub>2</sub>=H; R<sub>3</sub>=CH<sub>2</sub>OH}, C<sub>18</sub>H<sub>18</sub>O<sub>6</sub>            340 = {R<sub>1</sub>=OCH<sub>3</sub>; R<sub>2</sub>=H; R<sub>3</sub>=C<sub>3</sub>H<sub>5</sub>}, C<sub>20</sub>H<sub>20</sub>O<sub>5</sub></p>

	
<p>C) biphenyl</p> 	<p>246 = {R1=R2=H}, C<sub>14</sub>H<sub>14</sub>O<sub>4</sub>  260 = {R1=H, R2=CH<sub>3</sub>}, C<sub>15</sub>H<sub>16</sub>O<sub>4</sub>  272 = {R1=H; R2=C<sub>2</sub>H<sub>3</sub>}, C<sub>16</sub>H<sub>17</sub>O<sub>4</sub></p>

The depolymerisation of AL over Ni-Nb-SBA-15 for 3h led to compounds with molecular weight range from 105 to 800 Da (Fig. S4a) such as monomers (with dominant molecular mass signals, m/z of 162, 176, 192, 206, 222, 226, 242, 244), dimers (with dominant molecular mass signals, m/z of 246, 260, 272, 298, 312, 326, 340, 358, 360, 374, 446, 460) and some possible tri- and tetramers traces (m/z of 420 to 800 Da). This mass spectrum is very similar to that of AL pre-treated lignin depolymerized over Ni-SBA-15 for 6h (Fig S3b). By extending the reaction time, from 3 to 6 h, only identification of the monomeric compounds with m/z of 162, 222, 242, 244 and dimers (with significant peaks of 260, 272, 312, 326, 340, 358, 360, 374, 376 m/z) (Fig. S4b) was possible. On the other hand, the results obtained by HPSEC analysis due to increase in reaction time up to 6h did not maintain the same trend (Fig. 7) with those recorded by LDI-TOF-MS. As we observed in the previous study [54] the association of molecules during the HPSEC separation (i.e. hydrodynamic volume) could justify the difference between the results obtained by the two techniques aforementioned analysis techniques.

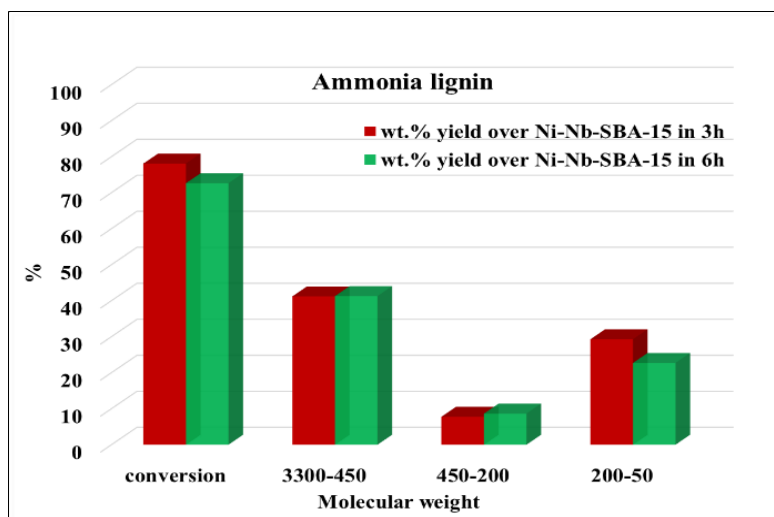


**Fig. 7** Depolymerisation of ammonia lignin under autoclave conditions (0.1g Ni-Nb-SBA-15, 0.5 g AL, 70 mL methanol, 50 bars H<sub>2</sub>, 180 °C).

The depolymerisation of lignin is a challenging process due to competitive repolymerization reactions. An important observation during these experiments was noticed after an increase in the amount of Ni-Nb-SBA-15 from 0.1 to 0.3 g which led to a decrease of conversion as well as of the yield in mono and dimers compounds (Fig. 8). Although Ni supported on acidic support as well as the hydrogenolysis process can suppress repolymerization [11] and, consequently, lead to an increase in catalytic performances, the increase in acid sites with the higher catalyst addition could lead to repolymerization of lignin intermediates [55]. Moreover, this aforementioned trend was also maintained for hydrogenolysis of formic acid lignin. Therefore, the depolymerisation of lignin over heterogeneous acid catalysts can be a challenging process due to the presence of competitive repolymerization reactions.

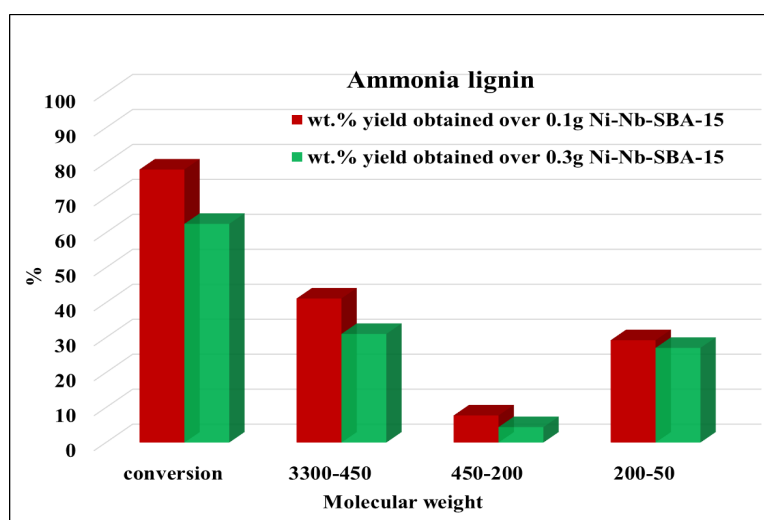


**Fig. 8** Depolymerisation of ammonia lignin under autoclave conditions (0.5 g AL, 70 mL methanol, 50 bars H<sub>2</sub>, 180 °C, 3h).

The catalytic cleavage of C–C bonds ( $\beta$ – $\beta$ ,  $\beta$ –1,  $\beta$ –5 and 5–5) which connected the monomeric units of lignin is more difficult to be carried out than for C–O bonds ( $\beta$ –O–4,  $\alpha$ –O–4, 4–O–5) [56]. As it was earlier mentioned the structure of FAL involves, mainly, both the C–C and C–O bonds (but not  $\beta$ –O–4) [24] between phenylpropan units. Its hydrogenolysis over Ni–(Nb)–SBA-15 led to high conversion but with low yield in mono or dimers (yield of 10 wt.%(Fig. 9), limited by robust C–C interunit linkages whose bond dissociation energy is very high as well as due to low content of  $\beta$ –O–4 [57].

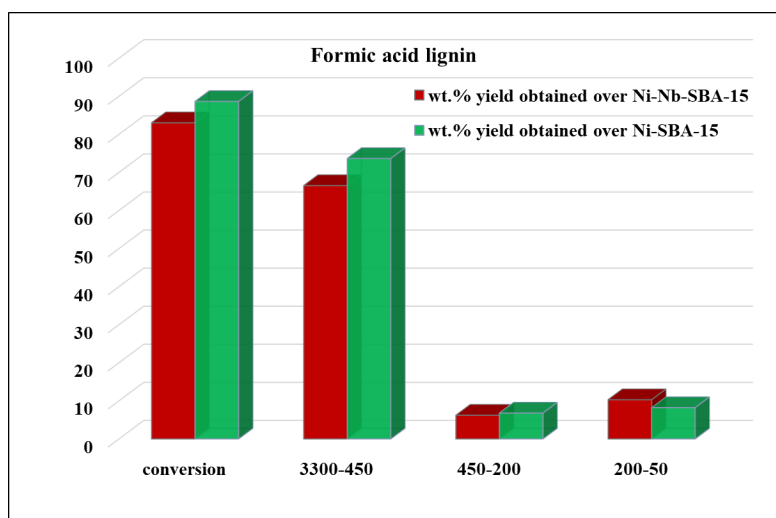
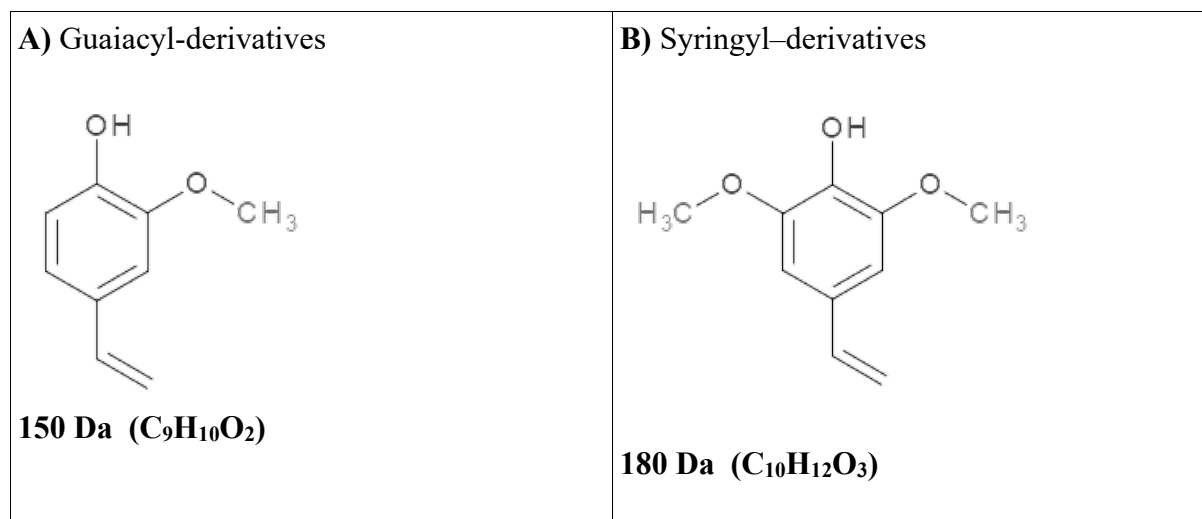


**Fig. 9** Depolymerisation of formic acid lignin under autoclave conditions (0.1g catalyst, 0.5 g FAL, 70 ml methanol, 50 bars H<sub>2</sub>, 180 °C, 6 h).

On the other hand, the increase in yield of monomers over Ni–Nb–SBA-15 in comparison with those obtained over Ni–SBA-15 (Fig. 9) was not as obvious as in case of AL (Fig. 6). Therefore, the cleavage of the C–O linkages between aromatic units of lignin, the activation of  $\beta$ –O–4 linkages on the Nb-based catalyst was most notable. The improving of catalytic selectivity to monomers, as result of Nb presence was also highlighted by LDI-TOF-MS analysis which showed, in the presence of Nb species, a decrease in intensity of the signals corresponding to the dimers (Fig. S5). Regarding the depolymerisation process of FAL sample over Ni–SBA-15 and Ni–Nb–SBA-15 catalysts for 6h, respectively, a similar distribution of related-monomeric (with m/z of 150, 162, 176, 180, 192, 206) and -dimeric (with m/z of 297, 312, 326, 340, 353) compounds was observed in the corresponding mass spectra (Fig. S5 a-b). Due to the heterogeneity of the lignin samples, a difference of 12-17 Da was observed between the adjacent peaks which is correlated to different numbers of O/C atoms and/or CH/CH<sub>2</sub>/OH

groups presented in the molecular structures [41,44]. The peaks at  $m/z$  of 150 and 180 correspond to compounds derived from G and S-unit, respectively, where a 4-vinyl moiety is present in the phenolic structure, as shown in Table 5.

**Table 5** Different possible type-structures of monomeric-related components from FAL lignin depolymerisation process, compared to AL lignin depolymerisation process (with their elemental compositions): A) Guaiacyl, B) Syringyl - derivatives



In addition, the mass spectra showed peaks at  $m/z$  of 107 and  $m/z$  of 112 that might be attributed to alkylphenols [58] and cyclotene [43], respectively as reported in the open literature. The peak at  $m/z$  of 144 correspond to an unknown compound (possibly to a polysaccharide fragment according to the open literature [59]). A low content of  $\beta$ -O-4 bonds in the FAL lignin sample [24] is pointed out by the low numbers of peaks detected in the mass spectra related to dimers fragments such as the  $m/z$  of 329 [49] and 383 peaks [60] compared to the corresponding mass spectra of AL lignin. Some possible trimers traces (with a significant peak at  $m/z$  of 507 corresponding to a GGG-type structure [61]) was observed on the spectra of FAL lignin when working with the Ni-SBA-15 catalyst.

Y. Cao *et al.* reported harsh conditions such as 6 MPa hydrogen pressure and temperatures of 230 °C for catalytic hydrogenolysis of cellulose to ethylene glycol over Ni-SBA-15 based catalysts [62] which is in accordance to lower conversion of AL compared with that for FAL over Ni-Nb-SBA-15 (Fig. 9) since the hydrogenolysis process of lignin is carried out in methanol and not in water. On the other hand, the higher yields in monomers obtained after depolymerisation of ammonia lignin over Ni-Nb-SBA-15 were due to a significant presence of  $\beta$ -O-4 linkage between its monomers (Fig. 10). Therefore, the type of linkage between the monomeric units of the lignin as well as the purity of lignin influenced the catalytic depolymerisation process.

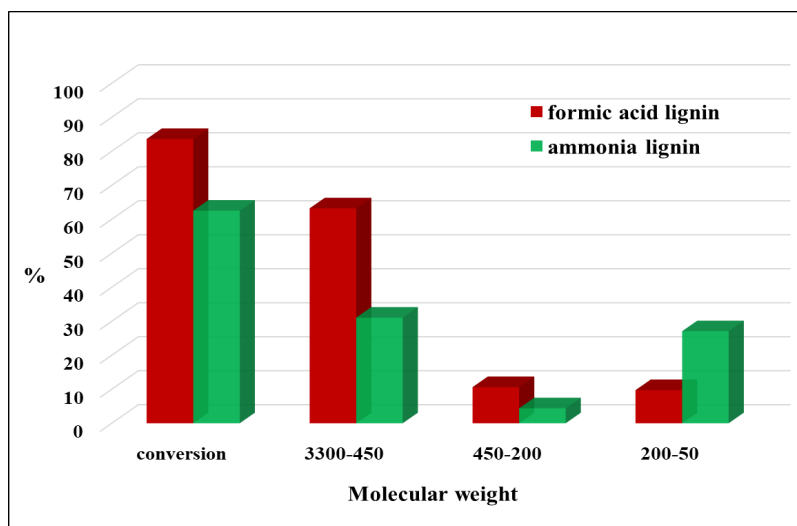


**Fig. 10** Depolymerisation of lignin under autoclave conditions over Ni-Nb-SBA-15 (0.1g catalyst, 0.5g lignin, 70 mL methanol, 50 bars H<sub>2</sub>, 180 °C, 6 h).

In view of these experiments, the catalytic stability of Ni-Nb-SBA-15 was evaluated both in terms of the hydrogenolysis of ammonia and of formic acid lignin. If Ni-Nb-SBA-15 catalyst showed a good stability during the three catalytic cycles in the hydrogenolysis of FAL (Fig. 11), for depolymerisation of AL a significant decrease in conversion of around 20% from first to third catalytic cycles was noticed (Fig. 12). The decrease of both conversion and yield in monomers was due to the chemisorption of sulphur, present in the unfractionated ammonia lignin as highlighted in the previous study [54], on active Ni sites [63].

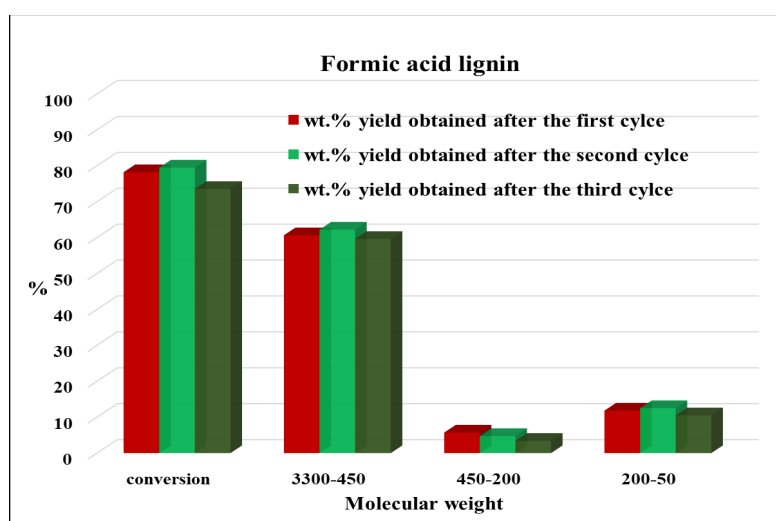


**Fig. 11** Catalytic stability of Ni-Nb-SBA-15 in the depolymerization of FAL under autoclave conditions (0.3g Ni-Nb-SBA-15, 0.5g lignin, 70 ml methanol, 50 bars H<sub>2</sub>, 180 °C, 3h).



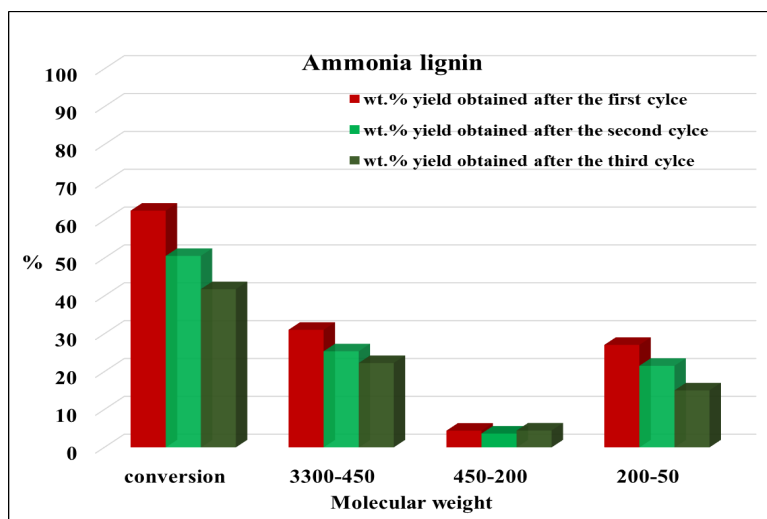


**Fig. 12** Catalytic stability of Ni-Nb-SBA-15 in the depolymerization of AL under autoclave conditions (0.3g Ni-Nb-SBA-15, 0.5g lignin, 70 ml methanol, 50 bars H<sub>2</sub>, 180 °C, 3h).

#### 4 Conclusions

The **hydrogenolysis** process of isolated lignin from Miscanthus plant under acidic or basic conditions was carried out over Ni and/or Nb-doped SBA-15 catalysts under autoclave conditions and the reaction products were **characterized** by several techniques such as LDI-TOF-MS, HPSEC and GC-MS. The predominance of  $\beta$ -O-4 ether bond between phenylpropane units from ammonia lignin as well as the synergistic effect between Ni and **acid sites represented by Nb** in the cleavage of C-O and C-C bonds led to the highest yield in monomers (22wt.%) as results of hydrogenolysis process. **Therefore, the presence of acid sites due to insertion of Nb into SBA-15 structure led to an improvement of catalytic performance in depolymerization of lignin.** On the other hand the presence of sulfur in the composition of AL affected the catalytic performances of Ni-Nb-SBA-15, these decreasing **along** the three catalytic cycles. **A very interesting aspect was noticed in the increase in amount of Ni-Nb-SBA-15 which did not lead to an improve of its catalytic performance in the depolymerisation of AL due to repolymerization process of lignin intermediates as a result of increase in the amount of acid sites.**

#### Conflicts of Interest

The authors declare no competing financial interest.

#### Acknowledgements

This work is also a part of activities of the Technical Chemistry, Department of Chemistry, Chemical-Biological Centre, Umeå University, Sweden as well as the Johan Gadolin Process Chemistry Centre at Åbo Akademi University in Finland. The Bio4Energy programme, the Wallenberg Wood Science Center (under auspices of the KAW foundation and Kempe Foundations are gratefully acknowledged.

## Author contributions

Ajaikumar Samikannug: methodology, validation, investigation, writing – review & editing; Alina Tirsoaga: writing–original draft, writing – review & editing; Vlad Tofan: investigation; Rodica Ganea: methodology; Jyri Pekka Mikkola: supervision, writing – review & editing, resources; Aurore Richel: supervision, writing – review & editing; Marian Nicolae Verziu: conceptualization, supervision, writing–original draft, writing – review & editing.

## References

1. Toledano A, Serrano L, Labidi J (2014) Improving base catalyzed lignin depolymerization by avoiding lignin repolymerization. *Fuel* 116: 617–624
2. Cheng C, Shen D, Gub S, Luo KH (2018) State-of-the-art catalytic hydrogenolysis of lignin for the production of aromatic chemicals. *Catal Sci Technol* 8: 6275-6296
3. Zakzeski J, Bruijninx PCA, Jongerius AL, Weckhuysen BM (2010) The Catalytic Valorization of Lignin for the Production of Renewable Chemicals. *Chem Rev* 110:3552–3599
4. Song QL, Zhao YP, Wu FP, Li GS, Fan X, Wang RY, Cao JP, Wei XY (2020) Selective hydrogenolysis of lignin-derived aryl ethers over Co/C@N catalysts. *Renew Energ* 148: 729-738
5. Hu J, Zhang S, Xiao R, Jiang X, Wang Y, Sun Y, Lu P (2019) Catalytic transfer hydrogenolysis of lignin into monophenols over platinum-rhenium supported on titanium dioxide using isopropanol as in situ hydrogen source. *Bioresour Technol* 279: 228-233
6. Monedero BG, Ruiza MP, Bimbela F, Faria J (2017) Selective hydrogenolysis of  $\alpha$ -O-4,  $\beta$ -O-4, 4-O-5 CO bonds of lignin-model compounds and lignin-containing stillage derived from cellulosic bioethanol processing. *Appl Catal A Gen* 541:60-76
7. Jeon W, Choi IH, Park JY, Lee JS, Hwang KR (2020) Alkaline wet oxidation of lignin over Cu-Mn mixed oxide catalysts for production of vanillin. *Catal Today* 352: 95-103
8. Mahmood N, Yuan Z, Schmidt J, Xu C (2015) Hydrolytic depolymerization of hydrolysis lignin: Effects of catalysts and solvents. *Bioresour Technol* 190: 416-419
9. Patwardhan PR, Brown RC, Shanks BH (2011) Understanding the Fast Pyrolysis of Lignin. *ChemSusChem* 4:1629-1636
10. Zhang J (2018) Catalytic transfer hydrogenolysis as an efficient route in cleavage of lignin and model compounds. *Green Energy Environ* 3: 328-334
11. Chen X, Guan W, Tsang CW, Hu H, Liang C (2019) Lignin Valorizations with Ni Catalysts for Renewable Chemicals and Fuels Productions. *Catalysts* 9: 488-526
12. McVeigh A, Bouxin FP, Jarvis MC, Jackson SD (2016) Catalytic depolymerisation of isolated lignin to fine chemicals: part 2 – process optimisation. *Catal Sci Technol* 6 : 4142–4150
13. Gao X, Zhu S, Li Y (2019) Selective hydrogenolysis of lignin and model compounds to monophenols over AuPd/CeO<sub>2</sub>. *Mol. Catal.*, 462, pp. 69-76
14. Zakzeski J, Weckhuysen BM (2011) Lignin Solubilization and Aqueous Phase Reforming for the Production of Aromatic Chemicals and Hydrogen. *ChemSusChem* 4: 369–378
15. Qin Y, Wang H, Ruan H, Feng M, Yang B (2018) High Catalytic Efficiency of Lignin Depolymerization over Low Pd-Zeolite Y Loading at Mild Temperature. *Front Energy Res* 6: 1-7
16. Li H, Song G (2019) Ru-catalyzed hydrogenolysis of lignin: base-dependent tunability of monomeric phenols and mechanistic study. *ACS Catal* 9: 4054–4064
17. Song Q, Wang F, Cai J, Wang Y, Zhang J, Yu W, Xu J (2013) Lignin depolymerization (LDP) in alcohol over nickel-based catalysts via a fragmentation–hydrogenolysis process. *Energy Environ Sci* 6 : 994–1007
18. Zhang J, Teo J, Chen X, Asakura H, Tanaka T, Teramura K, Yan N (2014) A Series of NiM (M = Ru, Rh, and Pd) Bimetallic Catalysts for Effective Lignin Hydrogenolysis in Water. *ACS Catal* 4: 1574-1583

19. Shao Y, Xia Q, Dong L, Liu X, Han X, Parker SF, Cheng Y, Daemen L L, Cuesta A J R, Yang S, Wang Y (2017) Selective production of arenes via direct lignin upgrading over a niobium-based catalyst. *Nat. Commun.* 8: Article 16104
20. Dong L, Xin Y, Liu X, Guo Y, Pao CW, Chen JL, Wang Y (2019) Selective hydrodeoxygenation of lignin oil to valuable phenolics over Au/Nb<sub>2</sub>O<sub>5</sub> in water. *Green Chem* 21: 3081-3090
21. Chen P, Zhang Q, Shu R, Xu Y, Ma L, Wang T (2017) Catalytic depolymerization of the hydrolyzed lignin over mesoporous catalysts. *Bioresour Technol* 226: 125–131
22. Thepparat K, Laosiripojana N, Cronin D, Moghaddam L, Zhang Z, Doherty WOS (2015) Effects of mesostructured silica catalysts on the depolymerization of organosolv lignin fractionated from woody eucalyptus. *Bioresour Technol* 180: 222–229
23. Song W, He Y, Lai S, Lai W, Yi X, Yang W, Jiang X (2020) Selective Hydrodeoxygenation of Lignin Phenols to Alcohols in Aqueous Phase over Hierarchical Nb<sub>2</sub>O<sub>5</sub>-Supported Ni Catalyst. *Green Chem* 22: 1662-1670
24. Vanderghem C, Richel A, Jacquet N, Blecker C, Paquot M (2011) Impact of formic/acetic acid and ammonia pre-treatments on chemical structure and physicochemical properties of *Miscanthus x giganteus* lignins. *Polym Degrad Stab* 96: 1761-1770
25. Zhao D, Huo Q, Feng J, Chmelka BF, Stucky GD (1998) Nonionic Triblock and Star Diblock Copolymer and Oligomeric Surfactant Syntheses of Highly Ordered, Hydrothermally Stable, Mesoporous Silica Structures. *J Am Chem Soc* 120: 6024-6036
26. Rahmat N, Abdullah AZ, Santra C, Mohamed AR (2010) A Review: Mesoporous Santa Barbara Amorphous-15, Types, Synthesis and Its Applications towards Biorefinery Production. *Amer J Appl Sci* 7: 1579-1586
27. Rahman S, Shah S, Santra C, Sen D, Sharma S, Pandey JK, Mazumder S, Chowdhury B (2016) Controllable synthesis of niobium doped mesoporous silica materials with various morphologies and its activity for oxidative catalysis. *Microporous Mesoporous Mater* 226 : 169-178
28. Peng K, Li X, Liu X, Wang Y (2017) Hydrothermally stable Nb-SBA-15 catalysts applied in carbohydrate conversion to 5-hydroxymethylfurfural. *Mol Catal* 441: 72-80
29. Kaneko K (1994) Determination of pore size and pore size distribution: 1. Adsorbents and catalysts. *J Membrane Sci* 96: 59-89
30. Zhang Y, Pan Z, Wang N, Wang L (2021) Performance of carbon-modified Pd/SBA-15 catalyst for 2-ethylanthraquinone hydrogenation. *Mol Catal* 504: 111424-111431
31. Jehng JM, Wachs IE (1991) Structural Chemistry and Raman Spectra of Niobium Oxides. *Chem Mater* 3: 100-107
32. Tesser R, Vitiello R, Carotenuto G, Sancho GC., Vergara A., Torres MPJ, Li C, Di Serio M (2015) Niobia supported on silica as a catalyst for Biodiesel production from waste oil. *Catal Sustain Energy* 2: 33–42
33. Rojas E, Delgado JJ, Pérezc MOG, Bañares MA (2013) Performance of NiO and Ni–Nb–O active phases during the ethane ammoxidation into acetonitrile. *Catal Sci Technol* 3: 3173-3182
34. Jin S, Xiao Z, Chen X, Wang L, Guo J, Zhang M, Liang C (2015) Cleavage of lignin-derived 4-O-5 aryl ethers over nickel nanoparticles supported on niobic acid-activated carbon composites. *Ind Eng Chem Res* 54: 2302–2310
35. Deepa A K, Dhepe P L (2015) Lignin depolymerization into aromatic monomers over solid acid catalysts. *ACS Catal* 1: 365–379
36. Sturgeon MR, O'Brien MH, Ciesielski PN, Katahira R, Kruger JS, Chmely SC, Hamlin J, Lawrence K, Hunsinger GB, Foust TD, Baldwin RM, Bidy MJ, Beckham GT(2014)Lignin depolymerisation by nickel supported layered-double hydroxide catalysts. *Green Chem* 16: 824-835
37. Kim JY, Park SY, Choi IG, Choi JW (2018) Evaluation of Ru<sub>x</sub>Ni<sub>1-x</sub>/SBA-15 catalysts for depolymerization features of lignin macromolecule into monomeric phenols. *Chem Eng J* 336: 640–648

38. Sergeev AG, Hartwig JF (2011) Selective, Nickel-Catalyzed Hydrogenolysis of Aryl Ethers. *Science* 332: 439-443
39. Kong L, Zhang L, Gu J, Gou L, Xie L, Wang Y, Dai L (2020) Catalytic hydrotreatment of kraft lignin into aromatic alcohols over nickel-rhenium supported on niobium oxide catalyst. *Bioresour Technol* 299:122582-122590
40. Cole DP, Smith EA, Lee YJ (2012) High-resolution mass spectrometric characterization of molecules on biochar from pyrolysis and gasification of switchgrass. *Energy Fuels* 26: 3803-3809
41. Saito SK, Kato T, Takamori H, Kishimoto T, Fkushima K (2005) A new analysis of the depolymerized fragments of lignin polymer using ToF-SIMS. *Biomacromolecules* 6: 2688-2696
42. Li J, Gellerstedt G (2008) Improved lignin properties and reactivity by modifications in the autohydrolysis process of aspen wood. *Ind. Crops Prod* 27: 175-181
43. Christensen E, Evans RJ, Carpenter D (2017) High-resolution mass spectrometric analysis of biomass pyrolysis. *J Anal Appl Pyrol* 124: 327-334
44. Banoub J, Delmas GH Jr., Joly N, Mackenzie G, Cachet N, Bouchra BM, Delmas M (2015) A critique on the structural analysis of lignins and application of novel tandem mass spectrometric strategies to determine lignin sequencing. *J Mass Spectrom* 50: 5-48
45. Hempfling R, Schulten HR (1990) Chemical characterization of the organic mater in forest soils by Curie point pyrolysis-GC/MS and pyrolysis-filed ionization mass spectrometry. *Org Geochem* 15: 131-145
46. Dong L, Xia J, Guo Y, Liu X, Wang H, Wang Y (2021) Mechanisms of Caromatic-C bonds cleavage in lignin over NbOx-supported Ru catalyst. *J Catal* 394: 94-103
47. Flaherty DW, Hibbitts DD, Iglesia E (2014) Metal-Catalyzed C-C Bond Cleavage in Alkanes: Effects of Methyl Substitution on Transition-State Structures and Stability. *J Am Chem Soc* 136: 9664-9676
48. Richel A, Vanderghem C, Simon M, Wathelet B, Paquot M (2012) Evaluation of matrix-assisted laser desorption/ionization mass spectrometry for second-generation lignin analysis. *Anal Chem Insights* 7: 79-89
49. Letourneau DR, Volmer DA (2021) Mass spectrometry-based methods for the advanced characterization and strutural analysis of lignin: A review. *Mass Spec Rev* 1-45
50. Kriger O, Budenkova E, Babich O, Suhih S, Patyukov N, Masyutin Y, Dolganuk V, Chupakhin E (2020) The process of producun bioethanol from delignified cellulose isolated from plants of the *Miscanthus* genus. *Bioengineering* 7: 61-71
51. Morreel K, Dima O, Kim H, Lu F, Niculaes C, Vanholme R, Dauwe R, Goeminne G, Inze D, Messens E, Ralph J, Boerjan W (2010) Mass Spectrometry-Based Sequencing of Lignin Oligomers. *Plant Physiol* 153:1464-1478
52. Yoshioka K, Watanabe T, Ando D (2011) A comparative study of matr- and Nano-assisted laser desorption/ionisation time-of-flight mass spectrometry of isolated and synthetic lignin. *Phytochem Anal* 23: 248-253
53. Bayerbach R, Nguyen VD, Schurr U, Meier D (2006) Characterization of water-insoluble fraction from fast pyrolysis liquids (pyrolytic lignin). Part III. Molar mass characteristics by SEC, MALDI-TOF-MS, LDI-TOF-MS and Py-FIMS. *J Anal Appl Pyrol* 77: 95-101
54. Verziu M, Tirsoaga A, Cojocar B, Bucur C, Tudora B, Richel A, Aguedo M, Samikannug A, Mikkola JP (2018) Hydrogenolysis of lignin over Ru-based catalysts: The role of the ruthenium in a lignin fragmentation process. *Mol Catal* 450: 65-76
55. Mei C, Hu C, Hu Q, Sun C, Li L, Liang X, Dong Y, Gu X (2020) Effective Depolymerization of Sodium Lignosulfonate over  $\text{SO}_4^{2-}/\text{TiO}_2$  Catalyst. *Catalysts* 10: 995
56. Mukundan S, Atanda L, Beltramini J (2019) Thermocatalytic cleavage of C-C and C-O bonds in model compounds and kraft lignin by NiMoS<sub>2</sub>/C nanocatalyst. *Sustain Energy Fuels* 3: 1317-1328

57. Shuai L, Sitison J, Sadula S, Ding J, Thies MC, Saha B (2018) Selective C-C Bond Cleavage of Methylenelinked Lignin Models and Kraft Lignin. *ACS Catal* 8:, pp. 6507–6512
58. Lucejko JJ, Tamburini D, Modugno F., Ribechini E, Colombini P (2021) Analytical pyrolysis and mass spectrometry to characterise lignin in archaeological wood. *Appl Sci* 11:240-275
59. Nierop KGJ, Bergen PF, Buurman P, van Lagen B (2005) NaOH and Na<sub>4</sub>P<sub>2</sub>O<sub>7</sub> extractable organic matter in two allophanic volcanic ash soils of the Azores Islands : a pyrolysis GC/MC study. *Geodema* 127: 36-51
60. Navarrete P, Pizzi A, Pasch H, Delmotte L (2012) Study on Lignin-Glyoxal Reaction by MALDI-TOF and CP-MAS 13 C-NMR. *J Adhes Sci Technol* 26: 1069-1082
61. Prothmann J, Spegel P, Sandahl M, Turner C (2018) Identification of lignin oligomers in Kraft lignin using ultra-high-performance liquid chromatography/high-resolution multiple-stage tandem mass spectrometry (UHPLC/HRMSn). *Anal Bioanal Chem* 410: 7803-7814
62. Cao Y, Wang J, Kang M, Zhu Y (2014) Efficient synthesis of ethylene glycol from cellulose over Ni-WO<sub>3</sub>/SBA-15 catalysts. *J Mol Catal A: Chem* 381:46-53
63. Lakhapatri SL, Abraham MA (2013) Sulfur poisoning of Rh–Ni catalysts during steam reforming of sulfur-containing liquid fuels. *Catal Sci Technol* 3: 2755-2760